

Molecular structure of cyanidin metal complexes: Al(III) versus Mg(II)

Laura Estévez · Nicolás Otero · Ricardo A. Mosquera

Received: 30 June 2010/Accepted: 16 September 2010/Published online: 30 September 2010
© Springer-Verlag 2010

Abstract Metal complexation by anthocyanins is a very efficient mechanism for protecting plants. While Mg is an essential metal for life, typically found bound to anthocyanins, Al interferes with the metabolism of the former. Density functional theory and the polarizable continuum model are used to study cyanin (the simplest anthocyanin bearing a catechol unit) complexes with Mg(II) and Al(III), considering different metal ligand stoichiometries. Results obtained for metal-binding energies indicate that Al(III) complexes are always more stable than those of Mg(II). Furthermore, reaction energies for the metal exchange process show that free Al(III) (hexaaquo complex) is always able to displace Mg(II). This displacement is more favored when the metal ligand ratio decreases. Thus, anthocyanins are implied in suppressing Al(III) toxicity by enabling its accumulation and reducing its migration to ecosystems. The characteristics of Al(III)–cyanidin and Mg(II)–cyanidin bonds are investigated using the quantum theory of atoms in molecules. We find these complexes are more stabilized by ion–dipole electrostatic interactions than by electron pair sharing, as predicted by the Hard and Soft Acids Theory. Globally, two factors increase the covalent character: replacement of Mg(II) by Al(III) and replacement of water by cyanidin ligands.

Keywords Metal exchange · Metal binding · Anthocyanidins · QTAIM · Electron delocalization indices · HSAB theory

1 Introduction

Flavonoids are aromatic secondary metabolites found ubiquitously in plants [1, 2]. These molecules are receiving renewed attention by many researchers during the last decade because of their remarkable array of biological and physiological effects [3–5], the complexity of their biosynthesis and metabolism, possible industrial applications, and constantly rising commercial interest and relevance in the processes involved in nutrition, flavors, and aromas [6, 7].

Structurally, anthocyanins are hydroxylated and methoxylated derivates of flavylium, 2-phenyl-1-benzopyrylium, salts. They are the most intensively colored group of flavonoids [1], being vacuolar pigments synthesized exclusively by organisms of the plant kingdom, and have been observed to occur in all tissues of higher plants, providing color in leaves, stems, flowers, and fruits [8]. The stability of the structure of these molecules in vivo, conditioning the stability of their color, is influenced by the number and the nature of the substituents, the pH value of the medium, soil composition, and climate conditions. Their stability is also partially improved by glycosylation and acylation, but it is very dependent upon possible copigmentation, self-association, and metal complexation reactions [9–14].

Formation of metal complexes by anthocyanins is important for diverse features: (1) it is a very sensitive and powerful mechanism for color stabilization developed in higher plants in vivo [1, 2]; (2) it is also one of the

Published as part of the special issue celebrating theoretical and computational chemistry in Spain.

L. Estévez · N. Otero · R. A. Mosquera (✉)
Departamento de Química Física, Universidade de Vigo,
Lagoas-Marcosende s/n, 36310 Vigo, Spain
e-mail: mosquera@uvigo.es

mechanisms that enable accumulation of metals in peripheral tissues reducing the possibility of their migration to eco systems suppressing metal toxicity [15–17]; (3) at the same time, metal complexation is a very efficient mechanism of protecting plants from pathogens and plant eaters; and (4) the antioxidative activity of flavonoids, besides the direct free radical scavenging, includes chelation reactions of diverse metal as well [18].

Our interest on Mg(II) and Al(III) complexes is due to two facts. On one hand, recently, Shiono et al. [19] determined for the first time the crystal structure of one anthocyanin copigment: protocyanin. This crystal structure mainly consists of cyanin molecules (cyanidin 3-O-(6-O-succinyl glucoside)-5-O-glucoside). One Mg(II) is coordinated bidentately to three different cyanin fragments through the catechol moiety of each cyanin, arranged (Fig. 1) in octahedral coordination geometry. On the other hand, Al(III) is found in its ionic form in most kinds of animal and plant tissues and in natural waters everywhere [15–17], being the third most prevalent element and the most abundant metal in the earth's crust. Al(III) occurs in most soils, but its availability to plants is highly pH dependent and most aluminum toxicity is reported in strongly acidic soils [15–17, 20, 21]. Moreover, it is known that Al(III) toxicity is among the most widespread problems of ion toxicity stress in plants so it interferes with the metabolism of essential metals like Mg(II) [22, 23].

We think that the geometry obtained for the crystal structure by Shiono et al. (Fig. 1) can be taken as a good starting point for our purpose. To the best of our knowledge, this is the first theoretical study on metal-anthocyanin complexes, and there is poor information about them. This

crystal structure leads us to consider diverse systems in order to study metal complexation of anthocyanins. This work does not only deal with both the theoretical study of metal exchange processes of Al(III) in cyanin–Mg(II) complexes, but with the description of metal–cyanin interactions through the characterization of metal–ligand bonds from an electronic point of view. The latter will be done using the quantum theory of atoms in molecules, QTAIM [24, 25], which has proved to provide chemists with a tool to interpret, understand, and predict diverse experimental observations [26].

2 Computational details

The geometry obtained from the X-ray diffraction study of the reconstructed protocyanin crystal [19], $C_{366}H_{233}O_{228}Ca_2FeMg$, whose residual and weighted R factors for the set of reflections judged as significantly intense were, respectively, 0.083 and 0.211, allowed us to extract an initial geometry for the models of metal complex studied in this work (Fig. 1). Thus, we have studied the following systems: metal, M, (Mg^{2+} or Al^{3+}) attached to one, two or three bidentate ligand/s, L, (cyanin). The global charge of each cyanin isolated ligand is -1 , as it could be obtained formally upon deprotonation of two hydroxyls ($3'$ and $4'$) of the corresponding cationic cyanin or cyanidin. Thus, cavities formed by ligand/s display charges of -1 , -2 and -3 in each of the complexes here studied.

The complex we extract from the crystal consists of 3 cyanins acting each one as a bidentate ligand linked to magnesium with global charge of -1 (Fig. 1). To construct

Fig. 1 Substructure extracted from the original crystal structure [19] showing the 1:3 Mg(II)-cyanin complex (before substituting glucoses by methyls). It is also shown the structural formula of cyanin and labeling of selected atoms for a better compression of the text

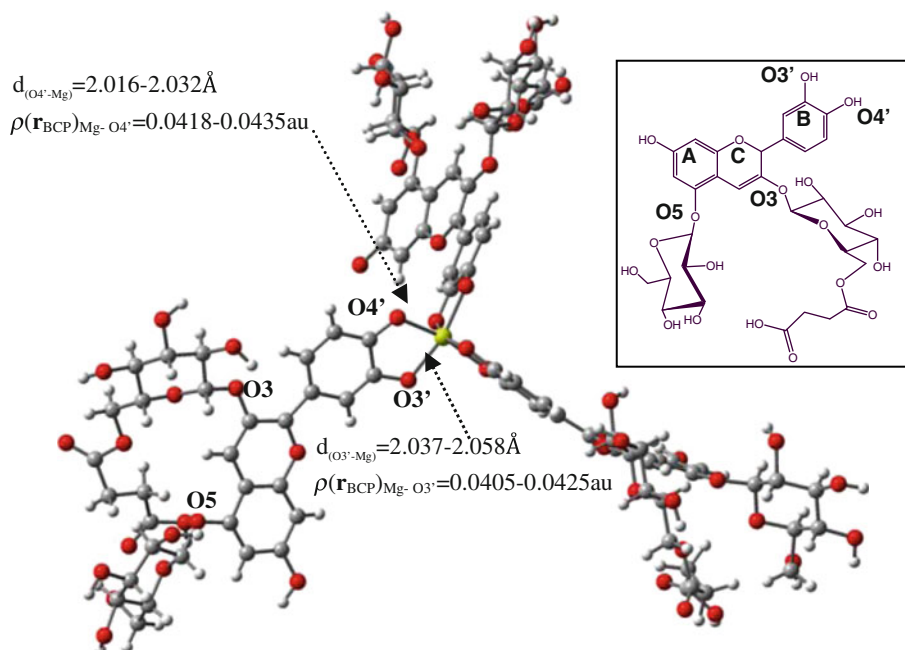
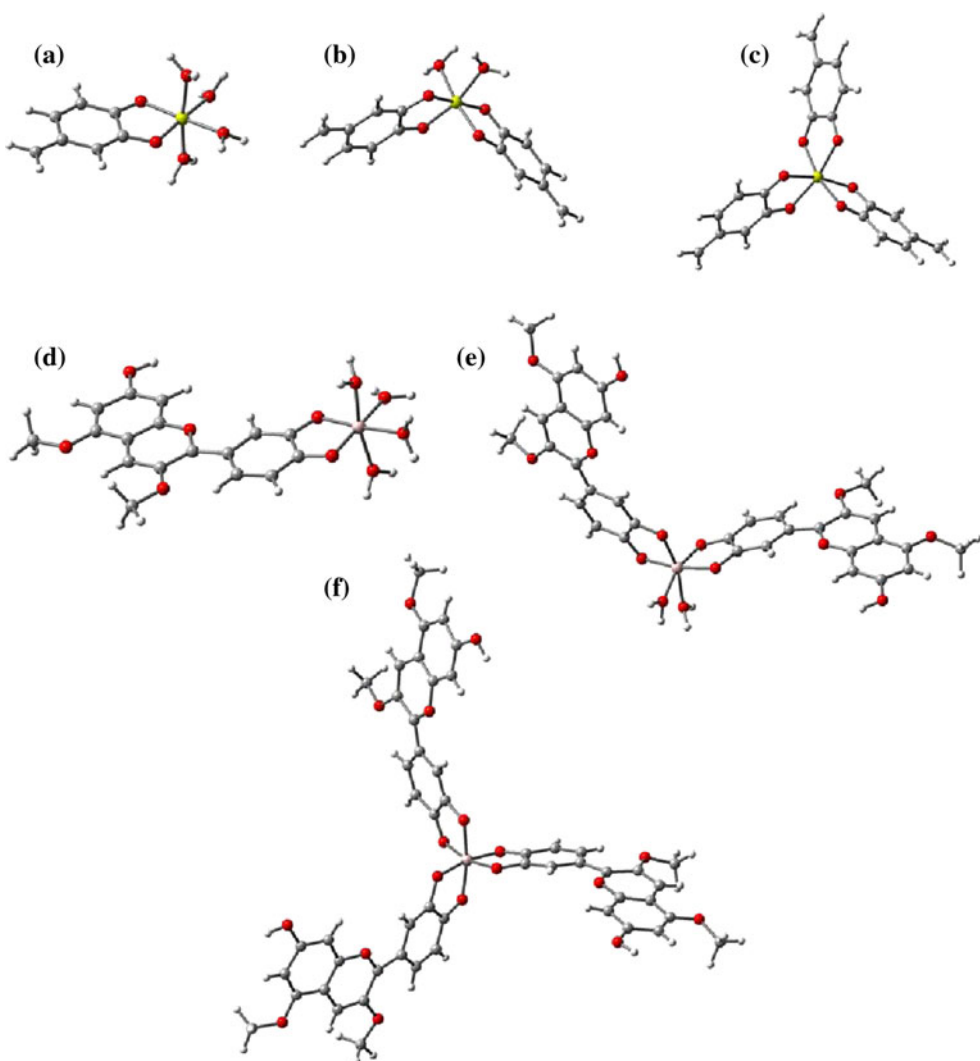


Fig. 2 1:1, 1:2, and 1:3 MgL' models (**a**, **b** and **c**, respectively), 1:1 complex in the optimized geometry in aqueous solution simulated with the PCM model (**d**), and the geometries studied for 1:2 and 1:3 AlCy complexes (**e** and **f**, respectively). Similar pictures were obtained for the corresponding 1:1, 1:2, and 1:3 MgCy complexes



the remaining magnesium complexes, with one or two ligands, we change one or two original cyanins by two or four water molecules, respectively. Because of the high computational cost involved, we have only performed complete optimization for 1:1 complexes. Both 1:2 and 1:3 complexes were computed with single point calculations at the same level (see below), where M–O distances, for ligands and water molecules, $M\text{--}O_L$ and $M\text{--}O_w$, were fixed at the values obtained in the optimization of model compounds, while the remaining geometry parameters are those of the crystal. Model compounds (Fig. 2a–c) were constructed replacing cyanin ligands by dideprotonated 3,4-dihydroxybenzyl cation, L', whose global formal charge is also –1. Furthermore, in this study, we can assume that the effect of the glucose substituents in the metal–ligand bond is negligible (see below). Thus, they were substituted for methyls in order to reduce the computational cost. The same procedure was done for aluminum complexes (Fig. 2d–f).

Comparison of 1:1 complexes obtained for MgL, MgL', AlL, and AlL' was used to estimate model reliability. We have seen that M–O bond distances with both ligands (L and L') and water follow the same behavior. They do never differ by more than 0.02 Å, excluding that of M–O_{4'} (0.05 Å), and they always follow the same relative order. Finally, the differences between Al–O and Mg–O bond lengths are nearly the same in the 1:1 complexes formed with L and L'.

All calculations were carried out with the Gaussian03 package [27]. It has already been established that density functional methods give reliable results in most chemical systems [28, 29]. Density Functional Theory (DFT)/Hartree–Fock (HF) hybrid methods are particularly appealing for the present investigation since they correct the pure DFT overestimation of the bond dissociation energies [30] as was validated by Johnson et al. [31]. We have chosen the B3LYP hybrid DFT approximate functional [32] for this work, which consists of the B3 exchange functional [33],

the LYP correlation functional [34], and a 20% of exact HF exchange. This density functional implementation has generally been shown to perform quite reliable results for most chemical systems, and the scope of this work is not out of the range where B3LYP have been extensively tested [35, 36].

Frequencies, the corresponding zero-point vibrational energy (ZPVE) corrections, thermal corrections to energy (E_{TRV}), and entropies at 298.15 K were calculated for 1:1 complexes at this level of theory using standard statistical mechanical expressions [37]. The enthalpy and Gibbs function changes for the complexation were evaluated at 298.15 K as follows:



$$\Delta_r H = \Delta_r E_{\text{elec}} + \Delta_r E_{\text{TRV}} + \Delta_r \text{ZPVE} + (2n - 1) RT$$

$$\Delta_r G = \Delta_r H - T\Delta_r S$$

Gas phase energies for 1:1 complexes were recalculated on the B3LYP/6-31++G(d,p) optimized geometries at the B3LYP/6-31++G(2df,2p) level of theory and corrected with the ZPVE and thermodynamical data calculated from the B3LYP/6-31++G(d,p) results. The energy of the remaining complexes was computed at the B3LYP/6-311++G(2df,2p) level on the non-optimized geometries described above.

Aqueous phase optimizations were carried out using the self-consistent reaction field method (SCRF), with the polarizable continuum model (PCM) [38–40] procedure at the B3LYP(PCM)/6-31++G(d,p) level. Solvation free energies were also recalculated at the B3LYP(PCM)/6-311++G(2df,2p) level of theory for 1:1 complexes, while the same procedure described above was employed for the rest of the complexes. Continuum models of solvation constitute one efficient way to include condensed-phase effects into quantum mechanical calculations, by means of using a self-consistent reaction field (SCRF) approach for the electrostatic component. Previously, it has been shown

that for the specific cases of Al(III) and Mg(II), PCM does yield reliable results [41]. Gas phase corrections were employed to estimate the aqueous phase thermodynamic properties as found in the literature [41, 42], since the calculation of vibrational frequencies in liquid phase is computationally demanding and not very accurate, and corrections are expected to be very similar [43, 44].

Finally, electron densities, $\rho(\mathbf{r})$, obtained at the B3LYP/6-311++G(2df,2p) level in both phases, were studied with QTAIM as implemented in the AIMPAC package [45]. We analyze the main properties of $\rho(\mathbf{r})$ evaluated at the bond critical points (BCPs), like its value, $\rho(\mathbf{r}_c)$, and atomic properties obtained by integrating $\rho(\mathbf{r})$ over atomic basins, Ω , as electron atomic population, $N(\Omega)$, and atomic energy, $E(\Omega)$, and their respective variations upon complex formation, $\Delta N(\Omega)$ and $\Delta E(\Omega)$. We mainly focus on BCPs involved directly in the metal–ligand bond paths, M–O_L. With regard to $\Delta N(\Omega)$, we focus on that of the metal, $N(M)$, those of oxygens of the ligand directly bound to the metal, $N(O_L)$, and those of oxygens of water molecules of the first hydrated shell of metal, $N(O_w)$. The accuracy obtained in the determination of the integrated properties was checked using standard criteria. Thus, all atoms considered were integrated with absolute values of $L(\Omega)$ [24, 25] below 2×10^{-3} au, and summations of atomic electron populations and atomic energies differ from those of the corresponding molecule always by less than 1.6×10^{-3} au and 1.7 kJ mol⁻¹, respectively.

3 Results

3.1 Energies

Molecular energies computed at the B3LYP/6-311++G(2df,2p)//B3LYP/6-31++G(d,p) level for both 1:1 metal–Cy complexes in both phases, as well as for ligand and hexahydrated metal ions are given in Table 1. For

Table 1 Gas phase and water solution molecular energies, E (in au) at the B3LYP/6-311++G(2df,2p)//6-31++G(d,p) level for 1:1 complexes, hydrated metals, ligand, and water

Optimized geometry	$E_{\text{elec}}^{\text{GAS}}$	$E_{\text{elec}}^{\text{PCM}}$	Crystal structure ^a	$E_{\text{elec}}^{\text{GAS}}$	$E_{\text{elec}}^{\text{PCM}}$
Cy:Mg (1:1)	−1613.27699	−1613.39383	Cy:Mg (1:1)	−1613.12414	−1613.24027
Cy:Al (1:1)	−1655.33601	−1655.61255	Cy:Al (1:1)	−1655.18768	−1655.44969
Mg(H ₂ O) ₆ ²⁺	−658.52467	−658.85606	Cy:Mg (2:1)	−2567.52694	−2567.63868
Al(H ₂ O) ₆ ³⁺	−700.29981	−701.02969	Cy:Al (2:1)	−2609.76671	−2609.88527
H ₂ O	−76.46257	−76.47178	Cy:Mg (3:1)	−3521.82607	−3522.03139
Cyanidin	−1107.34391	−1107.28203	Cy:Al (3:1)	−3564.17819	−3564.28997
			Cyanidin	−1107.17509	−1107.30831

For remaining complexes, molecular energies were obtained at the B3LYP/6-311++G(2df,2p) in both phases

^a See text for the description of the geometries

remaining complexes, those enclosing two or three bidentate cyanidins, molecular energies were obtained from single point calculations at the B3LYP/6-311++G(2df,2p) level (Table 1) on the geometries described above. For all stoichiometries, the most stable metal complex is that formed with Al(III) both in gas phase and in PCM modeled aqueous solution.

3.1.1 Metal-binding affinity

Metal-binding affinities of cyanidin to Mg(II) and Al(III) were evaluated by calculating the energy variation of the following reaction:



where x and y are the charges of the metal cation, L and M stand, respectively, for the bidentate ligand and the metal, and n corresponds to the number of cyanidins bound bidentately. This reaction defines the metal-binding affinity as the water/ligand substitution from the first hydration shell of the metal, where all the exchanges occur simultaneously.

Looking at Table 2, we notice there is a significant difference between binding energies obtained for optimized 1:1 M:Cy complexes and those obtained for 1:1 M:Cy in the geometry of the crystal. Nevertheless, we observed that the relative binding energy between Al:Cy and Mg:Cy with both geometries is very similar, e.g., it differs by less than 0.5 kcal mol⁻¹ in gas phase. This fact

Table 2 B3LYP/6-311++G(2df,2p) energies for metal binding affinity (in kcal mol⁻¹) for the diverse complexes studied here, in the gas phase and in water solution

	ΔE^{GAS}	ΔE^{PCM}
Cy:Mg (1:1) ^a	-210.81 ^b	-19.49 ^b
	-210.57 ^c	-19.25 ^c
	-204.91 ^d	-10.85 ^e
Cy:Al (1:1) ^a	-389.58 ^b	-46.28 ^b
	-388.92 ^c	-45.86 ^c
	-380.91 ^d	-35.12 ^e
Cy:Mg (1:1)	-219.34	-16.70
Cy:Al (1:1)	-400.31	-39.16
Cy:Mg (2:1)	-315.25	-42.31
Cy:Al (2:1)	-606.81	-88.09
Cy:Mg (3:1)	-346.12	-64.34
Cy:Al (3:1)	-708.17	-117.65

^a From fully optimized structures (see text)

^b From electronic energies corrected with ZPVE

^c ΔH including E_{TRV} at 298.15 K

^d ΔG values at 298.15 K

^e ΔG values at 298.15 K computed for PCM modeled aqueous solution

leads us to believe that our model is reliable enough to compare binding energies of all Al and Mg complexes.

From these values (Table 2), we observe that both metals display favorable binding affinities, Al(III) displaying always the most negative one in the same phase and stoichiometry. The complexation reaction seems to be driven primarily by favorable charge–charge interactions, between the positively charged metal complex and the negatively charged cavity that regulates this affinity (increasing with the charge in absolute value). This is particularly remarkable in the case of Al(III), where binding affinities go from -400.31 to -708.17 kcal mol⁻¹ in gas phase and from -39.16 to -117.65 kcal mol⁻¹ in solution. The evolution of binding affinities with the number of ligands is not homogenous as can be expected when considering the repulsions among negatively charged ligands in 1:2 and 1:3 stoichiometries. We also notice that binding energies are substantially reduced in solution with regard to gas phase, what can be related to the destabilization of bulky compounds by the contribution coming from cavitation energies, i.e., the M:Cy complexes with regard to the solvated uncoordinated ligands.

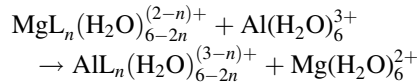
Consecutive ligand-binding energies, corresponding to the following reactions:



can be obtained as differences between values shown in Table 2. These differences indicate that increasing the number of cyanins leads always to more negative binding energies in both phases. Thus, the subsequent replacement of two water molecules by cyanin ligands is 39.16, 48.93 and 29.56 kcal mol⁻¹, respectively, for the first, second, and third replacement in $\text{Al}(\text{H}_2\text{O})_6^{3+}$ in aqueous solution. This qualitative trend is also true for Mg(II).

3.1.2 Metal exchange reaction

The metal exchange reaction is defined as follows:



The energy balance of this reaction, exchange energy, indicates the likelihood for hydrated Al(III) to replace a Mg(II) already attached to a binding site in a cyanidin molecule. In general, the exchange reaction is energetically very probable to occur from a thermodynamical point of view. In gas phase, it can be as favorable as 362.05 kcal mol⁻¹ (Table 3). The charge of the cavity plays a major role in the thermodynamics of the reaction. The more positive charge of Al(III) makes the exchange much more favorable as the ligand cavity becomes more negative. When solvation effects are included with PCM

Table 3 B3LYP/6-311++(2df, 2p) energies for metal exchange reaction (in kcal mol⁻¹) for the diverse complexes studied here, in the gas phase and in water solution

	ΔE^{GAS}	ΔE^{PCM}
Cy:Mg (1:1) → Cy:Al (1:1) ^a	-178.13 ^b	-28.93 ^b
	-178.35 ^c	-27.88 ^c
	-180.28 ^d	-25.53 ^e
Cy:Mg (1:1) → Cy:Al (1:1)	-180.97	-22.46
Cy:Mg (2:1) → Cy:Al (2:1)	-291.56	-45.78
Cy:Mg (3:1) → Cy:Al (3:1)	-362.05	-53.31

^a From fully optimized structures (see text)^b From electronic energies corrected with ZPVE^c ΔH including E_{TRV} at 298.15 K^d ΔG values at 298.15 K^e ΔG values at 298.15 K computed for PCM modeled aqueous solution

calculations, the exchange energy reduces drastically. This relates to the higher solvation energy of $\text{Al}(\text{H}_2\text{O})_6^{3+}$, compared to $\text{Mg}(\text{H}_2\text{O})_6^{2+}$.

3.2 Characterization of metal–cyanidin bonding

3.2.1 Characterization of metal–cyanidin bonding in terms of bond critical points

We remark that all $\rho(\mathbf{r}_c)$ values corresponding to M–L bonds are significantly smaller than those of usual covalent bonds and much larger than those displayed by closed-shell interactions (Tables 4, 5), as previously found in other metal complexes [46, 47]. Such values were classified by Bader in the low end for shared interactions [46]. Nevertheless, all $\nabla^2\rho(\mathbf{r}_c)$ values of M–L BCPs are small and positive, what has been considered as a hallmark of closed-shell interactions [48]. This combination of BCP indices, relatively low values for $\rho(\mathbf{r}_c)$, small positive values for $\nabla^2\rho(\mathbf{r}_c)$, and small negative values for the total energy density at the BCP (data not shown), coupled with significant electron delocalization (see below) has been considered unique to bonding to a metal atom [49–51]. In general, the interatomic surface for all the metal interactions falls in the region of the outer shell of charge depletion of the metal atom. This imparts to metal bonding the above described hallmarks.

The main properties of $\rho(\mathbf{r})$ evaluated at the metal–ligand, M–L, BCPs for 1:1 Cy–Mg complexes (Table 4) built with and without *O*-glucose substituents show that the presence of these groups has no significant effect on the properties of these bonds. In fact, the largest difference between $\rho(\mathbf{r}_c)$ values does not exceed 2×10^{-5} au.

Comparing M–O_L bond lengths in the optimized geometry of 1:1 MgCy complex and in the geometry

extracted from the crystal structure, we notice that the longest bonds are Mg–4' O_L in the former (by 0.045 Å) and Mg–3' O_L for the latter (by 0.026 Å) (Fig. 1; Table 4). Moreover, all M–O_L distances obtained from the simpler models provided the same trend: shorter M–3' O_L (with higher $\rho(\mathbf{r}_c)$ values) and longer M–4' O_L (with lower $\rho(\mathbf{r}_c)$ values) bond lengths. Differences in M–O_L bond lengths with regard to those found in the crystal structure could be due to crystal structure packing. Even stacking interactions with other polyphenols responsible of the final structure of the crystal [19] may affect the behavior of O_L.

Comparing both 1:1 optimized Al:Cy and Mg:Cy complexes, we notice that the former shows shorter M–O_L and M–O_w bonds than the latter (Tables 4, 5). This tendency is observed for the remaining stoichiometries studied, due to the weaker electrostatic interaction between the lower-charged Mg(II) and the ligands when compared with Al(III), and also due to the bigger ionic radius of the former.

Water molecules included in complexes are placed at distances from M obtained from our optimized simpler models and span in the range indicated in Tables 4 and 5. In all cases, these distances are longer than M–O_L ones and display smaller $\rho(\mathbf{r}_c)$ values. According to $\rho(\mathbf{r}_c)$ values, a clear trend can be established where M–O_L and M–O_w bond strength of both Al(III) and Mg(II) complexes reduces as the number of ligands increases. Moreover, these M–O_w distances are always larger than in the corresponding hexaaquo complexes. Thus, metal–cyanin bonds are reinforced undermining metal–water ones.

As far as the variation of the main properties of BCPs in atoms of cyanidin implied in metal complexation (Table 6), we also observed, as one could be expected, that C–O3' and C–O4' bonds in B ring shorten and C3'–C4' lengthen as a consequence of bonding to Mg(II). The same is true for Al(III) where variations are larger. Correspondingly, where bonds shorten $\rho(\mathbf{r}_c)$ values increase and where bonds lengthen they decrease.

3.2.2 Atomic electron population analysis

The analysis of QTAIM atomic electron populations, $N(\Omega)$, reveals that both cyanidin and metals are altered significantly upon metal binding. Cyanidin loses an important amount of electron density upon complexation (more than 0.2 au). It is remarkable that the electron density lost by cyanidin is removed from its AC bicyclic, which loses 0.682 au upon formation of 1:1 MgCy, while the B ring electron density enlarges significantly (0.481 au). In MgCy[−] formation, most of the electron density taken from AC is provided by the carbon atoms of this cycle (0.449 au), whereas that lost by their attached hydrogens (0.126 au), the methyl groups replacing *O*-glycoside units

Table 4 B3LYP/6-311++G(2df,2p) electron density, $\rho(\mathbf{r}_c)$, and its laplacian, $\nabla^2\rho(\mathbf{r}_c)$, in au multiplied by 10^3 and by 10^2 , respectively, for the BCPs found between metal, M, and ligand, O_L, (cyanidin) in optimized complexes

System	BCP	GAS			PCM		
		$10^3\rho(\mathbf{r}_c)$	$10^2\nabla^2\rho(\mathbf{r}_c)$	R	$10^3\rho(\mathbf{r}_c)$	$10^2\nabla^2\rho(\mathbf{r}_c)$	R
Mg(H ₂ O) ₆ ²⁺	M–O _W	32.5	21.84	2.110	34.9	24.14	2.082
Al(H ₂ O) ₆ ³⁺	M–O _W	56.9	32.13	1.942	62.5	37.80	1.902
Cy:Mg (1:1)	M–O _{W_up}	28.1	17.65	2.179	29.8	19.11	2.154
	M–O _{W_dw}	28.1	17.64	2.179	29.7	19.06	2.155
	M–O _{W_O3'}	32.1	21.23	2.119	32.6	21.53	2.116
	M–O _{W_O4'}	31.6	21.92	2.105	33.7	23.25	2.092
	M–3'O _L	51.0	35.37	1.986	45.3	30.59	2.025
	M–4'O _L	45.2	30.31	2.031	40.7	26.83	2.064
	M–O _{W_up}	44.3	23.34	2.034	51.2	28.12	1.983
Cy:Al (1:1)	M–O _{W_dw}	44.3	23.34	2.034	51.5	29.74	1.968
	M–O _{W_O3'}	50.1	27.32	1.988	55.2	31.31	1.952
	M–O _{W_O4'}	50.8	29.56	1.968	58.0	34.38	1.927
	M–3'O _L	92.1	57.92	1.794	81.8	49.06	1.836
	M–4'O _L	90.8	56.44	1.800	77.7	45.64	1.855
	M–O _{W_up}	27.7	17.52	2.179	30.3	19.12	2.154
Cy:Mg (1:1) ^a	M–O _{W_dw}	28.4	17.78	2.179	30.4	19.46	2.155
	M–O _{W_O3'}	32.9	21.41	2.119	33.3	21.78	2.116
	M–O _{W_O4'}	31.8	22.22	2.105	34.6	23.72	2.092
	M–3'O _L	50.9	35.53	1.986	45.6	30.77	2.025
	M–4'O _L	45.2	30.00	2.031	40.9	26.82	2.064
	M–O _{W_up}	44.4	23.30	2.034	51.1	28.46	1.983
Cy:Al (1:1) ^a	M–O _{W_dw}	46.0	23.30	2.034	55.0	30.12	1.968
	M–O _{W_O3'}	51.4	27.55	1.988	56.7	31.70	1.952
	M–O _{W_O4'}	50.5	29.76	1.968	57.2	34.61	1.927
	M–3'O _L	92.7	58.40	1.794	82.0	49.15	1.836
	M–4'O _L	90.7	56.41	1.800	77.8	45.65	1.855
	M–O _{W_up}	27.7	17.52	2.179	—	—	—
Cy:Mg (1:1) ^b	M–O _{W_dw}	28.4	17.78	2.179	—	—	—
	M–O _{W_O3'}	32.9	21.41	2.119	—	—	—
	M–O _{W_O4'}	31.8	22.22	2.105	—	—	—
	M–3'O _L	50.9	35.53	1.986	—	—	—
	M–4'O _L	45.2	30.00	2.031	—	—	—

They are compared with $\rho(\mathbf{r}_c)$ of the BCP between M and the oxygen of water molecules, O_W. Internuclear distances, R, in Å are also shown

^a From single point calculation (see text for geometry description)

^b From single point calculations on the same geometry, but replacing methyls by glucose substituents with the same geometry characteristics as in the crystal

(0.087 au), 7-OH (0.029 au), and O1 (which increases its electron population by 0.011 au), are much smaller. Global variations of electron populations in AC and B systems indicate that 70% of the electron density removed from AC is transferred to ring B. Nevertheless, this transference does not affect all the atoms of ring B. In fact, only those atoms directly involved in metal binding (O3' and O4' and the corresponding carbon atoms, C3' and C4') increase their electron populations (Fig. 1; Table 7), whereas the

remaining atoms also lose electron density (0.247 au in MgCy).

We can also observe that the metal atom is not the main electron density acceptor, e.g., Mg(II) only receives 0.029 au upon MgCy formation, as most of the electron density removed from cyanidin goes to the four water molecules attached to Mg(II) (0.104 au in total, that is 0.026 au per water molecule) and to the two water molecules expelled from Mg(H₂O)₆²⁺, which recover 0.029 au

Table 5 B3LYP/6-311++G(2df,2p) electron density, $\rho(\mathbf{r}_c)$, and its laplacian, $\nabla^2\rho(\mathbf{r}_c)$, in au multiplied by 10^3 and 10^2 , respectively, for the BCPs found between metal, M, and ligand, O_L, (cyanidin) in complexes with diverse stoichiometries

Complex ^a	BCP	GAS			PCM		
		$10^3\rho(\mathbf{r}_c)$	$10^2\nabla^2\rho(\mathbf{r}_c)$	R	$10^3\rho(\mathbf{r}_c)$	$10^2\nabla^2\rho(\mathbf{r}_c)$	R
Cy:Mg (2:1)	M–O _{W(dw}	28.1	18.67	2.159	31.1	19.75	2.146
	M–O _{W_O4'}	23.2	15.72	2.194	29.0	19.68	2.138
	M–3' O _{L1}	41.7	30.04	2.031	43.7	29.53	2.035
	M–4' O _{L1}	32.5	21.09	2.128	32.3	19.75	2.152
	M–3' O _{L2}	41.6	29.70	2.032	42.2	28.68	2.043
	M–4' O _{L2}	32.9	20.37	2.138	34.4	21.14	2.131
Cy:Mg (3:1)	M–3' O _{L1}	42.1	28.05	2.049	41.3	27.65	2.054
	M–4' O _{L1}	28.0	16.18	2.208	30.3	18.17	2.175
	M–3' O _{L2}	42.1	28.06	2.049	41.9	27.62	2.054
	M–4' O _{L2}	28.6	16.26	2.208	30.9	18.41	2.175
	M–3' O _{L3}	42.7	28.18	2.049	42.1	27.68	2.054
	M–4' O _{L3}	28.8	16.37	2.208	31.2	18.36	2.175
Cy:Al (2:1)	M–O _{W(dw}	42.3	21.05	2.063	50.4	27.17	1.995
	M–O _{W_O4'}	40.5	22.79	2.038	52.2	28.76	1.980
	M–3' O _{L1}	80.6	48.54	1.840	76.4	45.33	1.858
	M–4' O _{L1}	65.9	36.80	1.915	62.4	33.93	1.936
	M–3' O _{L2}	79.2	48.84	1.839	73.4	43.57	1.869
	M–4' O _{L2}	64.6	34.09	1.929	62.5	33.04	1.939
Cy:Al (3:1)	M–3' O _{L1}	73.5	44.11	1.866	71.5	42.57	1.876
	M–4' O _{L1}	52.2	25.81	2.005	54.4	27.78	1.987
	M–3' O _{L2}	72.5	43.85	1.866	70.3	41.95	1.879
	M–4' O _{L2}	52.1	25.65	2.006	54.8	27.87	1.986
	M–3' O _{L3}	73.0	44.06	1.867	70.6	42.07	1.880
	M–4' O _{L3}	52.8	25.93	2.005	55.0	27.94	1.987

They are compared with $\rho(\mathbf{r}_c)$ of the BCP between M and the oxygen of water molecules, O_W. Internuclear distances, R, in Å, are also shown

^a From single point calculation (see text for geometry description)

Table 6 Variation of the main properties of BCPs in atoms surrounding M–O_L bond, due to 1:1 metal complexation

	BCP	GAS			PCM		
		$\Delta\rho(\mathbf{r}_c)$	$\Delta H(\mathbf{r}_c)$	ΔR	$\Delta\rho(\mathbf{r}_c)$	$\Delta H(\mathbf{r}_c)$	ΔR
Mg:Cy(1:1)	C3'–O3'	-0.0641	0.14054	0.081	-0.0201	0.04545	0.026
	C3'–C4'	0.0363	-0.05737	-0.076	0.0523	-0.09815	-0.117
	C4'–O4'	-0.0519	0.10549	0.064	-0.0235	0.04863	0.029
Al:Cy(1:1)	C3'–O3'	-0.0885	0.19611	0.112	-0.041	0.06994	0.051
	C3'–C4'	0.0539	-0.08979	-0.111	0.0345	-0.05843	-0.067
	C4'–O4'	-0.0948	0.20072	0.121	-0.051	0.10864	0.065

Table 7 Variation of selected atomic properties: electron atomic population, $\Delta N(\Omega)$, and atomic energy, $\Delta E(\Omega)$, upon binding computed with B3LYP/6-311++G(2df,2p) electron densities in cyanin–metal complexes (in au multiplied by 10^3 but $\Delta E(M)$ in kcal mol⁻¹)

Compound	$\Sigma_L \Delta N(\Omega^L)$	$\Delta N(C3')$	$\Delta N(C4')$	$\Delta N(O3')$	$\Delta N(O4')$	$\Delta N(M)$	$\Delta E(M)$
Cy:Mg (1:1)	-201	266	213	119	130	29	-122.65
Cy:Al (1:1)	-274	361	398	159	183	41	-251.43

The summation of $\Delta N(\Omega)$ experienced by the atomic basins of the ligand, $\Sigma_L \Delta N(\Omega^L)$, is also shown

each. Looking at $N(\Omega)$ values in $\text{Mg}(\text{H}_2\text{O})_6^{2+}$, we notice that Mg(II) keeps a substantial positive charge in both coordination complexes, +1.79 in the former and +1.76 in $\text{MgCy}(\text{H}_2\text{O})_4^+$.

The electron density reorganization involved in cyanidin complexation to Al(III) is very similar to that described for Mg(II). We just notice that the electron density transferred from cyanidin is somewhat larger (Table 6). Although Al(III) receives more electron density than Mg(II), again, it is not the main electron density receptor, as the four water molecules in $\text{AlCy}(\text{H}_2\text{O})_4^{2+}$ increase their electron population in 0.025 au each (nearly the same amount observed in the Mg(II) complex), and the other two water molecules recover 0.065 au each, as they were attached to a more electropositive atom in $\text{Al}(\text{H}_2\text{O})_6^{3+}$. Again, electron density lost by cyanidin is mainly taken from the AC system and only accumulates on C and O atoms directly involved in metal bonding. Also, Al(III) keeps a substantial positive charge in both coordination complexes (+2.61 in $\text{Al}(\text{H}_2\text{O})_6^{3+}$ and +2.57 in the final complex).

Overall, we notice that global charge transference from ligand to metal is far from that usually assumed in some qualitative models. Water molecules included in 1:1 complexes are also electron density receptors, gaining even more electron density than the coordinated metal.

3.2.3 Characterization of metal–cyanidin bonding in terms of localized and shared electron pairs

As was indicated above, it has been claimed that one of the hallmarks of metal bonding is the coexistence of values of BCP properties that could be interpreted as due to closed-shell interactions, rather low $\rho(\mathbf{r}_c)$ values and small positive values for $\nabla^2\rho(\mathbf{r}_c)$, with significant electron delocalization, shown by rather large 2-center delocalization indices [52], $\delta(\Omega, \Omega')$, e.g., $\delta(\text{Cr}, \text{C})$ is 0.825 au in $\text{Cr}(\text{CO})_6$ and $\delta(\text{Ni}, \text{C})$ is 0.976 au in $\text{Ni}(\text{CO})_4$ [46]. Nevertheless, we notice in this case, $\delta(\text{M}, \text{O})$ values are significantly smaller (Table 8), falling out of the range usually observed for covalent bonds, pointing to these complexes are more stabilized by electrostatic interactions than by electron pair sharing, as predicted by the Hard and Soft Acids and Bases theory (HSAB) [53, 54].

Computation of localization indices, $\lambda(\Omega)$, and $\delta(\Omega, \Omega')$ indices allow to obtain the delocalized electron population for each atomic basin, $N^{\text{del}}(\Omega)$, as $N^{\text{del}}(\Omega) = [\Sigma_{\Omega'}\delta(\Omega, \Omega')]/2$. Thus, we notice the whole electron density transferred from ligands to M is completely employed as shared electron density, as $N^{\text{del}}(\Omega)$ exceeds the total amount of charge transference [$N(\Omega) - (Z_{\Omega} - x)$], where Z_{Ω} is the atomic number of Ω and x its formal oxidation state. Moreover, the metal shares a small amount of its initial electron density with the ligands (0.077 au in both Mg(II) optimized complexes and 0.047 au in Al(III) ones).

Table 8 Main parameters (in au) obtained from two-center electron delocalization analysis of B3LYP/6-311++G(2df,2p) optimized complexes

System	$\lambda(\text{M})$	$\delta(\text{M}, \text{O}_w)$	$\delta(\text{M}, \text{O}_L)$	$\delta(\text{M}, \Omega^x)$	$N^{\text{del}}(\text{M})$	$N(\text{M})$
$\text{Mg}(\text{H}_2\text{O})_6^{2+}$	9.921	0.090	–	0.002 ^c	0.280	10.203
$\text{Al}(\text{H}_2\text{O})_6^{3+}$	9.951	0.142	–	0.002 ^c	0.440	10.392
Cy:Mg (1:1)	9.918	0.088	0.127 ^a	0.003 ^d	0.308	10.231
			0.136 ^b			
Cy:Al (1:1)	9.949	0.117	0.235 ^a	0.006 ^d	0.479	10.433
			0.228 ^b			

^a $\text{M}-\text{O}3'$

^b $\text{M}-\text{O}4'$

^c Ω^x represents water hydrogens

^d Average for $\delta(\text{M}, \text{O}3')$ and $\delta(\text{M}, \text{O}4')$ indices

Relative values of $\delta(\text{M}, \text{O})$ indicate electron sharing with water ligands, and Cy is always larger with Al(III) than with Mg(II). Also, $N^{\text{del}}(\text{M})$ increases more from Mg(II) to Al(III) than $\lambda(\text{M})$, $\Delta N^{\text{del}}(\text{M})$ representing 84% of the increase in electron population experienced when Mg(II) is replaced by Al(III). Thus, although both complexes are basically formed by ion–dipole interactions, Al(III) gains more electron density from the ligands than Mg(II) because of the increase in the minority covalent character of M–O bonds.

The replacement of two water molecules by bidentate Cy results in larger $\delta(\text{M}, \text{O}_L)$ indices, while those of the remaining water molecules decrease (Table 8). Overall, $N^{\text{del}}(\text{M})$ increases because of this replacement. This increase is nearly equivalent to that experienced by the total electron population of the metal, $N(\text{M})$ (0.028 au for Mg(II) and 0.039 au for Al(III)). Thus, M–O bonds have a more covalent character when established with Cy oxygens than with water oxygens. Overall, we could say that the minority covalent character of M–O bonds is increased by two factors: replacement of Mg(II) by Al(III) and replacement of H_2O by Cy.

We also notice that replacement of water by Cy stabilizes the metal, as shown by $\Delta E(\text{M})$ values in Table 7. Furthermore, the difference between this quantity for Mg(II) and Al(III) (128 kcal mol⁻¹) represents 72% of metal exchange reaction energy (Table 6). This is the largest of the atomic contributions to metal exchange reaction energy, followed by C4' and C3' (-84.6 and -45.0 kcal mol⁻¹, respectively), and with those of O4' and O3' and water molecules the only significant negative ones, as most of the remaining atoms display positive contributions to this reaction energy, e.g., the set of carbons in the AC system display 86.8 kcal mol⁻¹. At least, two factors may be involved to explain the metal exchange reaction: (1) larger ability of Al(III) to polarize ligands and (2) larger

sharing of electron density in Al(III)-O_L bonds. Further calculations are planned to assess the relative weight of both contributions.

4 Conclusions

According to our B3LYP/6-311++G(2df,2p) calculations for the metal-cyanidin complexation, binding energies show that Al(III) complexes are always more favored than those of Mg(II), from a thermodynamical point of view. This is also confirmed by the reaction energies for metal exchange process.

QTAIM analysis reveals that cyanidin loses an important amount of electron density (more than 0.2 au) upon metal complexation that is transferred to the metal and coordinated water molecules. The source for this electron transfer is AC bicycle, while the part of B ring directly involved in complexation also increases its electron density.

We also conclude that both complexes are basically formed by ion-dipole interactions. Nevertheless, there is a minority covalent character in M-O bonds, which is larger in Al(III) complexes than in Mg(II) ones. This leads to Al(III) gains more electron density from the ligands than Mg(II).

Acknowledgments Authors thank “Centro de Supercomputación de Galicia” (CESGA) for free access to its computational facilities and the Galician Government for funding this research through project INCITE09E1R3141091ES.

References

1. Harborne JB (1976) Functions of flavonoids in plants. In: Goodwin TW (ed) Chemistry and biochemistry of plant pigments. Academic Press, London, pp 736–778
2. Harborne JB, Grayer R (1988) The anthocyanins, in the flavonoids. In: Harbone JB (ed) Advances in research since 1980. Chapman and Hall, London, pp 1–20
3. Cody V, Middleton E Jr, Harborne JB (1986) Plant flavonoids in biology and medicine: biochemical, pharmacological, and structure-activity relationships. Alan R. Liss Inc., New York
4. Harborne JB, Williams CA (1998) Nat Prod Rep 15:631–652
5. Harborne JB, Williams CA (1995) Nat Prod Rep 12:639–657
6. Wrolstad RE (2000) Anthocyanins. In: Lauro GJ, Francis FJ (eds) Natural food colorants. Science and technology. Marcel Dekker Inc., New York, pp 237–252
7. Andersen OM (2006) Flavonoids: chemistry, biochemistry and applications. CRC Press, Boca Raton
8. Robards K, Antolovich M (1997) Analyst 122:11R–34R
9. Dangles O, Saito N, Brouillard R (1993) Phytochemistry 34:119–124
10. Figueiredo P, Elhabiri M, Saito N, Brouillard R (1996) J Am Chem Soc 118:4788–4793
11. Mazzaracchio P, Pifferi P, Kindt M, Munyanza A, Barbioli G (2004) Int J Food Sci Technol 39:53–59
12. Ito F, Tanaka N, Katsuki A, Fujii T (2002) J Photochem Photobiol A Chem 150:153–157
13. Bayer E, Egger H, Fink A, Nether K, Wegmann K (1996) Angew Chem Int Ed Engl 5:791–798
14. Elhabiri M, Figueiredo P, Toki K, Saito N, Brouillard R (1997) J Chem Soc Perkin Trans 2:355–362
15. Matsumoto H (2000) Int Rev Cyt 200:1–46
16. Rout GR, Samantaray S, Das P (2001) Agronomie 21:3–21
17. Bartlett RJ, Riego DC (1972) Plant Soil 37:419–423
18. Cao G, Sofic E, Prior RL (1997) Free Radical Biol Med 22(5):749–760
19. Shiono M, Matsugaki N, Takeda K (2005) Nature 436:791
20. Pilon-Smits E, Pilon M (2002) Crit Rev Plant Sci 21:439–456
21. Schreiber HD, Swink AM, Godsey TD (2010) Inorg Biochem 104:732–739
22. Kiss T, Hollosi M (2001) The interaction of aluminum with peptides and proteins. In: Exley C (ed) Aluminum and Alzheimer's disease. Elsevier, Amsterdam
23. Kiss T, Gajda-Schrantz K, Zatta PF (2006) The Role of Aluminum in Neurotoxic and Neurodegenerative Processes. In: Sigel A, Sigel H, Sigel R (eds) Neurodegenerative diseases and metal ions. Wiley, England, pp 371–393
24. Bader RFW (1990) Atoms in molecules, a quantum theory. Oxford University Press, New York
25. Bader RFW (1991) A quantum theory of molecular structure and its applications. Chem Rev 91:893–928
26. Matta CF, Boyd RJ (2007) The quantum theory of atoms in molecules. Wiley, Darmstadt
27. Frisch MJ, Trucks GW, Schlegel HB, Scuseria GE, Robb MA, Cheeseman JR, Montgomery JA Jr, Vreven T, Kudin KN, Burant JC, Millam JM, Iyengar SS, Tomasi J, Barone V, Mennucci B, Cossi M, Scalmani G, Rega N, Petersson GA, Nakatsuji H, Hada M, Ehara M, Toyota K, Fukuda R, Hasegawa J, Ishida M, Nakajima T, Honda Y, Kitao O, Nakai H, Klene M, Li X, Knox JE, Hratchian HP, Cross JB, Bakken V, Adamo C, Jaramillo J, Gomperts R, Stratmann RE, Yazyev O, Austin AJ, Cammi R, Pomelli C, Ochterski JW, Ayala PY, Morokuma K, Voth GA, Salvador P, Dannenberg JJ, Zakrzewski VG, Dapprich S, Daniels AD, Strain MC, Farkas O, Malick DK, Rabuck AD, Raghavachari K, Foresman JB, Ortiz JV, Cui Q, Baboul AG, Clifford S, Cioslowski J, Stefanov BB, Liu G, Liashenko A, Piskorz P, Komaromi I, Martin RL, Fox DJ, Keith T, Al-Laham MA, Peng CY, Nanayakkara A, Challacombe M, Gill PMW, Johnson B, Chen W, Wong MW, Gonzalez C, Pople JA (2004) Gaussian 03, Revision E.01. Gaussian, Inc., Wallingford
28. Labanowsky J, Andzelelm J (1991) Density functional methods in chemistry. Springer, New York
29. Alcamí M, Mo O, Yáñez M (2001) Mass Spectr Rev 20:195–245
30. Tschinke V, Ziegler T (1991) Theor Chim Acta 81:65–78
31. Johnson BG, Gill PMW, Pople JA (1993) J Chem Phys 98:5612–5626
32. Stephens PJ, Devlin FJ, Chabalowski CF, Frisch MJ (1994) J Phys Chem 98:11623–11627
33. Becke AD (1993) J Chem Phys 98:5648–5652
34. Lee C, Yang W, Parr RG (1988) Phys Rev B 37:785–789
35. Merceiro JM, Matxain JM, Lopez X, York DM, Largo A, Eriksson LA, Ugalde JM (2005) Int J Mass Spectr 240:37–99
36. Kaltsosannis N, McGrady JE (2004) Principles and applications of density functional theory in inorganic chemistry II. Springer, Berlin
37. McQuarrie DA (1976) Statistical mechanics. Harper and Row, New York
38. Cancès E, Mennucci B, Tomasi J (1997) J Chem Phys 107: 3032–3041
39. Cossi M, Barone V, Mennucci B, Tomasi J (1998) Chem Phys Lett 286:253–260

40. Cancès E, Mennucci B, Tomasi J (1998) *J Chem Phys* 109:260–266
41. Mercero JM, Matxain JM, Rezabal E, Lopez X, Ugalde JM (2004) *Int J Quantum Chem* 98:409–424
42. Tunega D, Haberhauer G, Gerzabek M, Lischka H (2000) *J Phys Chem A* 104:6824–6833
43. Rezabal E, Mercero JM, Lopez X, Ugalde JM (2006) *J Inorg Biochem* 100:374–384
44. Rezabal E, Mercero JM, Lopez X, Ugalde JM (2007) *J Inorg Biochem* 101:1192–1200
45. Bader RFW (1994) AIMPAc: a suite of programs for the theory of atoms in molecules. Mc Master University, Hamilton
46. Cortés-Guzmán F, Bader RFW (2005) *Coord Chem Rev* 249:633–662
47. Stegmann R, Frenking G (1996) *Can J Chem* 74:801–809
48. Bone RGA, Bader RFW (1996) *J Phys Chem* 100:10892–10911
49. Molina JM, Dobado JA, Heard GL, Bader RFW, Sundberg MR (2001) *Theor Chem Acc* 105:365–373
50. Macchi P, Sironi A (2003) *Coord Chem Rev* 238:383–412
51. Macchi P, Proserpio DM, Sironi A (1998) *J Am Chem Soc* 120:13429–13435
52. Fradera X, Austen MA, Bader RFW (1999) *J Phys Chem A* 103:304–314
53. Pearson RG (1963) *J Am Chem Soc* 85:3533–3539
54. Pearson RG (1966) *Science* 151:172–177